

# Wind Farms in Weak Grids Stability Enhancement: SynCon or STATCOM?

Li Bao, Lingling Fan\*, Zhixin Miao

\**Department of Electrical Engineering, University of South Florida, Tampa FL USA 33620.*

*Phone: 1(813)974-2031, Email: linglingfan@usf.edu.*

---

## Abstract

Reactive power compensation is an effective method to enhance the stability of a power system. Synchronous condenser (SynCon) and static synchronous compensator (STATCOM) are widely used for reactive power compensation. They have the capability of increasing system stability and efficiency by absorbing or generating reactive power. This paper presents a comparison of SynCon and STATCOM under the condition of zero reactive power injection. The two devices are integrated into a grid-connected type-4 wind farm to examine their effects on system stability. It is found that SynCon is more capable in stability enhancement compared to STATCOM. To explain the difference, we measure the  $dq$ -frame admittance frequency-domain responses of the two devices using frequency scans. Vector fitting method is then utilized to convert the admittance frequency-domain measurements to an  $s$ -domain model. The  $s$ -domain admittance-based eigenvalue analysis further confirms that SynCon is advantageous in stability enhancement. The difference of SynCon and STATCOM can be summarized as SynCon providing a steady-state reactance while STATCOM acting as a current source at steady state.

*Keywords:* Reactive power compensation, synchronous condenser, STATCOM, wind farm

---

## 1. Introduction

Increasing penetrations of renewable energy sources such as wind farms have caused unexpected dynamic issues worldwide. In real-world operation, subsynchronous oscillations have been observed in the past decade in Texas, California, and China [1]. One type of oscillations is classified as weak grid oscillations by the IEEE PES Wind SSO task force report [1]. The low short circuit ratio (SCR) at the interconnection point is a factor that contributes to the oscillations. The mechanism of instability is similar as the traditional voltage stability: When wind power exporting level increases, the interconnection point voltage may decrease, as analyzed in [2, 3]. The decrease in the ac voltage can cause a decrease in the exporting power; thus, an

9 instability feedback mechanism is formed. Low SCR or weak grid interconnection makes this mechanism 9  
10 dominant and thus the system goes unstable [2, 3]. 10

11 In order to enhance voltage stability, reactive power compensation is an effective method. SynCon and 11  
12 STATCOM are two major devices for reactive power compensation. The objective of this paper is to compare 12  
13 the two devices in weak grid oscillation stability enhancement. 13

### 14 1.1. *SynCon and STATCOM* 14

15 SynCon have been applied in power systems for a very long. A reference in 1911 [4] presents the common 15  
16 applications of synchronous condenser at that time. Essentially, a synchronous condenser is a synchronous 16  
17 machine without a prime mover, working at motor operation. It is controlled by the excitation system 17  
18 to absorb or generate reactive power based on the requirement of power system. By the end of 2018, 90% 18  
19 of total generation capacity in Texas Panhandle area is wind generation. In order to enhance the stability 19  
20 and transmission efficiency, in April 2018, Electric Reliability Council of Texas (ERCOT) installed two 20  
21 synchronous condensers with rated capacity as +175/-125 MVA at the 345 kV substations in Panhandle, 21  
22 resulting in a 13% increase of power transfer compared that in of Year 2017 [5]. Reference [6] describes 22  
23 the project of installing four synchronous condensers with 13.8 kV at Vermont Electric Power Company 23  
24 (VELCO)'s Granite 230/115 kV station in Williamstown Vermont. This upgrade project improved the 24  
25 reliability and stability of the Vermont power grid. 25

26 In recent decades, STATCOMs also have been widely utilized with the development of switching devices 26  
27 such as IGBT and GTO [7]. A STATCOM consists of a voltage source converter and a capacitor, which 27  
28 is capable of regulating reactive power transfer to the power system and the local voltage. Compared to 28  
29 a synchronous condenser, STATCOM does not involve a rotating machine. It becomes the major reactive 29  
30 power device in the market. For example, in May 2001, the VELCO commissioned a project involving a 30  
31 STATCOM-based compensation system, which has a rated capacity of +133/-41 MVA, at Essex 115 kV 31  
32 station [8]. 32

33 Even though both SynCon and STATCOMs are vastly installed by utility companies, SynCon has been 33  
34 used more in islanded power grids, e.g., Kauai of Hawaii, as shown in [9], and in zones with low SCR, e.g., 34  
35 South Australia [10]. Apart from reactive power compensation, SynCon is used to enhance grid strength 35  
36 and provide inertia and fault currents. 36

37 In this paper, we show that SynCon is more advantageous for weak grid stability enhancement. 37

## 1.2. Study approaches

Both electromagnetic transient (EMT) simulation and eigenvalue analysis are employed in this research to examine SynCon and STATCOM's performance for a type-4 wind farm with weak grid interconnection.

For eigenvalue analysis, we adopt  $s$ -domain admittance-based eigenvalue analysis. This method was proposed by Semleyn in 1999 [11] and has been found applications for inverter-based resource stability analysis recently [12]. The benefit of this approach is that we no longer need to derive a state-space model. Rather, we can obtain admittance model through measurements. This feature is especially useful for EMT simulation models. For example, the STATCOM model employed in this study is a 48-pulse GTO-based model. State-space modeling approach requires derivation of an average model in a dq-frame. On the other hand, this step is saved by utilizing measurements.

By applying a voltage harmonic disturbance at the device's terminal with a range of frequency and measuring the excited current response at desired frequency, the frequency-domain measurement of an admittance can be obtained. To obtain an  $s$ -domain model or a transfer function from the frequency-domain response data, frequency-domain data fitting is required. Several packages of frequency-domain data fitting are available for use, e.g., the vector fitting package [13].

The objective of the vector fitting method is to fit a transfer function (matrix) to the frequency-domain measurements. The transfer function's order should be specified and the  $s$ -domain expression will be found. This can be done by minimizing the error between the measurement data and the frequency-response of the transfer function through iteratively tuning the parameters of the transfer function, e.g., poles and residues. In the end, a transfer function in  $s$ -domain can be found.

The vector fitting package in MATLAB is available in the public domain. In addition, MATLAB's system identification toolbox also offers tools, e.g., `tfest`, to estimate a transfer function from the frequency-domain response data [14].

With the  $s$ -domain admittances, eigenvalue analysis can be carried out for stability analysis.

## 1.3. Our contributions

There exists a large amount of literatures on comparison of SynCon and STATCOM. Reference [15] reviews the state-of-the-art reactive power compensation and their applications. The principles of operation and structures are also presented. Reference [16] demonstrates that SynCon and STATCOM have the similar dynamic performance at an HVDC system when subjected to a fault. Reference [17] proposes an inertial control for STATCOM, which provides better frequency response over SynCon.

68 In order to investigate the stability performance of STATCOM, [18] establishes the  $dq$ -domain small- 68  
69 signal impedance model of STATCOM by considering the phase-locked-loop (PLL) and other control loops, 69  
70 while reference [19] proposes the impedance model by injecting  $dq$ -domain perturbations. The two references 70  
71 determine the stability criterion through the Nyquist plots. 71

72 The aforementioned literatures treat SynCon and STATCOM as reactive power compensation devices, 72  
73 which enhance the stability dynamic by regulating reactive power to the system. This paper investigates 73  
74 whether a SynCon or a STATCOM can improve the system stability for zero reactive power injection. We 74  
75 found that SynCon can improve stability while STATCOM has limited impact on the system under such 75  
76 condition. In our preliminary work [20], we present EMT study. In this paper, we present an explanation by 76  
77 comparing the  $dq$ -frame admittance measurements of the two devices. The frequency-domain measurements 77  
78 are obtained through harmonic injection or frequency scans. From the frequency-domain measurement 78  
79 data, the  $s$ -domain admittance model is obtained by vector fitting method [13]. Eigenvalue analysis based 79  
80 on  $s$ -domain admittance confirms the EMT simulation results. 80

#### 81 *1.4. Structure of this paper* 81

82 This paper is organized as follows. Section II presents the EMT simulation results of a type-4 wind 82  
83 farm in a weak grid. The marginal stability condition is found through the EMT simulation. Furthermore, 83  
84 a SynCon or a STATCOM is integrated into the system to examine its effect. Section III presents the 84  
85  $dq$ -admittance frequency-domain measurements of the wind farm, STATCOM, and SynCon derived from 85  
86 harmonic injection. The  $s$ -domain models are also approximated by vector fitting of the measurements. 86  
87 Eigenvalue analysis results corroborate the EMT simulation results. This section also explains why there 87  
88 is a significant difference in stability enhancement through a comparison of the STATCOM and SynCon 88  
89 admittance models. Section IV concludes this paper. 89

## 90 **2. EMT Simulation Results** 90

91 This section will introduce the EMT testbeds and simulation result comparison for STATCOM and 91  
92 SynCon in a wind farm system. 92

### 93 *2.1. Wind farm* 93

94 The investigated system is a type-4 wind farm connected to a grid through a transmission line. Fig. 1 94  
95 presents the structure of the system. The terminal voltage of wind farm is 575 V. The wind farm is connected 95  
96 to the 220-kV transmission system via two step-up transformers. The reactive power devices are connected 96

97 to the grid through a 22-kV/220-kV transformer. The grid transmission network is comprised of two parallel 97  
 98 lines. A circuit breaker is shown and switching on/off of the breaker changes the total transmission network 98  
 99 impedance. 99

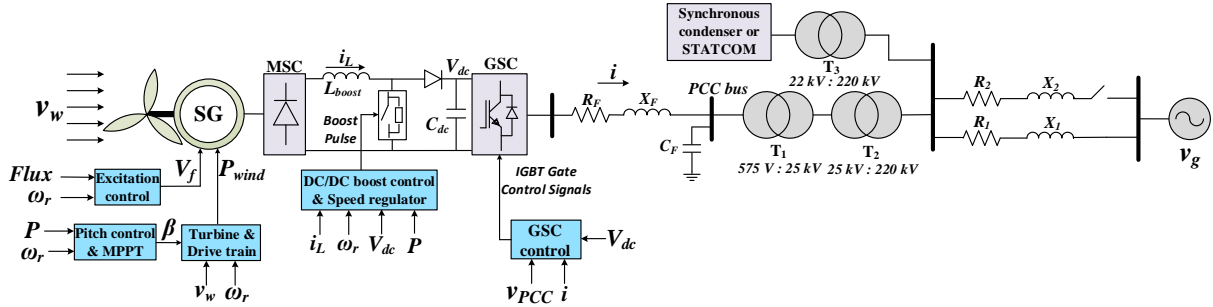


Figure 1: EMT testbed structure of a type-4 wind farm with reactive power devices.

100 The type-4 wind farm is constituted by a synchronous machine, a machine side converter (MSC) and 100  
 101 a grid side converter (GSC), which is connected to PCC through a choke filter. The GSC consists of 101  
 102 an inner current control loop and outer voltage control loops, as shown in Fig. 2. The inner current 102  
 103 controller generates the  $dq$ -frame voltage references, which will be further converted into the three-phase 103  
 104 voltage references relying on a synchronized phase angle provided by a phase-locked-loop (PLL). The outer 104  
 105 controllers are PCC voltage and DC-link voltage control. Since the PLL's d-axis is aligned with the PCC 105  
 106 voltage's space vector, the  $d$ -axis PCC voltage  $v_d$  has the same magnitude as  $V_{PCC}$  and  $v_q$  keeps as zero at 106  
 107 steady state. In the  $dq$ -frame, the expressions of active power and reactive power delivered from the GSC 107  
 108 to the grid are: 108

$$\begin{aligned} P &= v_d i_d \\ Q &= -v_d i_q \end{aligned} \quad (1)$$

109 Hence, to regulate active power, the  $d$ -axis current can be adjusted; while the  $q$ -axis current can be adjusted 109  
 110 for reactive power control. In addition, due to the relationship in (1), it can be seen that the active power 110  
 111 related control should employ negative feedback control while the reactive power or ac voltage control should 111  
 112 adopt positive feedback control. 112

Assuming that there is no converter power loss, the DC-link capacitor dynamics can be expressed as follows:

$$\frac{C_{dc}}{2} \frac{dV_{dc}^2}{dt} = P_{wind} - P \quad (2)$$

113 where  $P_{wind}$  is the total power injection from the wind turbine to the dc-link capacitor and the GSC. 113

114 Equation (2) illustrates the  $d$ -axis current order  $i_d^*$  can be generated by DC-link voltage control. Due to 114  
 115 the DC-link voltage relationship and the active power  $P$ , its can be seen that a positive feedback should be 115  
 116 employed for DC-link voltage control. The  $dq$ -axis current orders ( $i_{dq}^*$ ) for inner controller are from outputs 116  
 117 of the dc and ac voltage controllers. The parameters of wind farm and controller are listed in Table 1. 117

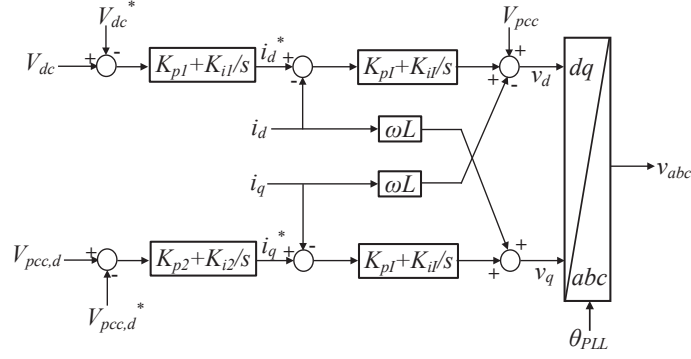


Figure 2: GSC control structure. The dc and ac voltage references are set at 1 pu.

Table 1: Parameters of the type-4 wind farm

Description	Parameters	Value (SI)
Rated Power	$P_{Rated}$	100 MW
Rated voltage	$V_{Rated}$	575 V
Nominal freq.	$f_{nom}$	60 Hz
DC-link voltage	$V_{DC}$	1100 V
Converter filter	$L_1, R_1$	0.06 mH, 0.45 mΩ
Shunt capacitor	$C$	90 mF
Stator winding reactance	$R_s, X_{ls}$	1.44 mΩ, 40.8 mΩ
Synchronous reactances	$X_d, X_q$	313 mΩ, 114 mΩ
Transient reactance	$X'_d$	71 mΩ
Subtransient reactances	$X''_d, X''_q$	60.5 mΩ, 58.3 mΩ
Open-circuit time constant	$T'_{do}, T''_{do}$	4.49 s, 0.0681 s
Short-circuit time constant	$T''_q$	0.0513 s
Inertia constant, poles	H, p	0.62, 2
Friction factors	F	0.01
Current PI controller	$k_{pi}, k_{ii}$	0.4, 48
DC voltage PI controller	$k_{p,dc}, k_{i,dc}$	1, 100
AC voltage PI controller	$k_{p,ac}, k_{i,ac}$	0.25, 25
PLL	$k_{p,PLL}, k_{i,PLL}$	60, 4480

## 118 2.2. STATCOM 118

119 STATCOM is widely adopted in power system to maintain voltage profile and enhance voltage stability 119  
 120 by offering additional reactive power. STATCOM consists of a DC capacitor and a voltage source converter, 120  
 121 which is connected to a grid through a transformer, as shown in Fig. 3(a). 121

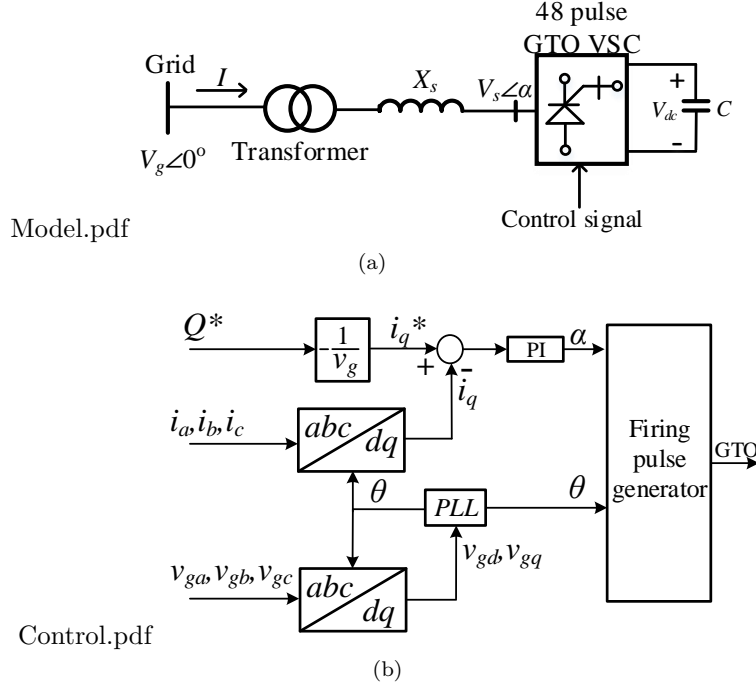


Figure 3: (a) Single-line diagram circuit of STATCOM. (b) Reactive power control block diagram of STATCOM.

The transferred active power ( $P$ ) and reactive power ( $Q$ ) from the grid to the STATCOM are controlled by adjusting the output voltage of the converter.  $P$  and  $Q$  can be represented as:

$$Q = \frac{|V_g|(|V_g| - |V_s| \cos \alpha)}{X_s} \quad (3)$$

$$P = |V_g||V_s| \frac{\sin(-\alpha)}{X_s} \quad (4)$$

122 where  $V_g$  is grid side voltage as  $1 \angle 0^\circ$ ,  $|V_s|$  and  $\alpha$  are the amplitude and phase angle of STATCOM's terminal 122  
 123 voltage. 123

124 According to (3) and (4), it can be concluded that the amount of transferred  $Q$  is controlled by adjusting 124  
 125 the magnitude of the STATCOM terminal voltage and  $P$  is controlled by adjusting the phase angle. Since 125  
 126 the STATCOM is used to offer reactive power, the phase angle between sending and receiving end is zero 126  
 127 at steady state. Hence, when the STATCOM voltage is lower than grid side, the grid sends reactive power 127  
 128 to the STATCOM. Otherwise, the STATCOM sends reactive power to the grid. 128

129 The STATCOM tested in this paper uses a voltage source converter built of four 12-pulse three-level 129  
 130 GTO inverters. Its detailed model is available in the demo of MATLAB/SimScape [21]. This model is 130  
 131 developed by P. Giroux and G. Sybille of Hydro-Quebec. Fig. 4(f) shows the multi-stepped output line- 131

132 to-line voltage of the 48-pulse GTO STATCOM. The zigzag phase-shifting transformers are connected to 132  
133 the VSC terminals. A simplified block diagram of the reactive power control is shown in Fig. 3(b) [22]. 133  
134 The instantaneous three-phase terminal voltage is used to generate the reference angle  $\theta$  through a PLL. 134  
135 Line current  $i$  is decomposed into real and reactive current, and the reactive current  $i_q$  is compared with 135  
136 the reference reactive current  $i_q^*$  to produce an angle  $\alpha$ , which defines the phase angle difference between 136  
137 converter output voltage and grid side voltage. Since the PLL aligns the grid voltage to  $d$ -axis,  $v_q$  is kept 137  
138 as 0, then  $Q = -i_q V_g$ . The reference reactive current can be generated from reference reactive power  $Q^*$ . 138

139 The magnitude and phase angle of the converter voltage determine the real and reactive power transferred 139  
140 between grid and STATCOM. If the STATCOM is only used for reactive power compensation, then the phase 140  
141 angle  $\alpha$  is kept close to 0 ( a small degree is for active power flow to compensate transformer loss), and 141  
142 reactive power is controlled by the voltage magnitude, which is directly proportional to capacitor voltage 142  
143  $V_{dc}$ . 143

144 If the STATCOM aims to increase its reactive power to the grid, or the grid aims to decrease its reactive 144  
145 power to the STATCOM,  $V_{dc}$  should increase and the phase angle  $\alpha$  should reduce to allow real power 145  
146 flowing from the grid to the STATCOM to charge the DC-link capacitor. The control logic in Fig. 3(b) 146  
147 shows that increasing  $Q^*$  causes a reduced  $i_q^*$  and  $\alpha$  will be subject to reduction initially. 147

148 Fig. 4 presents the dynamic performance of the STATCOM during operation. At  $t = 2$  s, the STATCOM 148  
149 increases its reactive power supply to the grid from 0 pu to 0.4 pu. This change causes the angle of STATCOM 149  
150 voltage  $\alpha$  to have a drop so that real power can be injected to the STATCOM to increase the capacitor 150  
151 voltage  $V_{dc}$ . The increased  $V_{dc}$  leads to a higher STATCOM output voltage  $V_s$  to realize reactive power 151  
152 generation. At  $t = 4$  s, the STATCOM reverses its reactive power command to absorbs 0.4 pu reactive 152  
153 power from grid. In turn, its dc-link voltage and ac voltage reduce. The phase angle  $\alpha$  is subject to change 153  
154 during transients but remains at around 0 at steady state. 154

155 Besides the reactive power control mode, STATCOM can also use terminal voltage control mode, as 155  
156 shown in Fig. 5. 156

The grid-side three-phase voltage  $v_{ga}$ ,  $v_{gb}$  and  $v_{gc}$  are converted into  $dq$ -frame, and its magnitude is calculated as:

$$V_g = \sqrt{V_{gd}^2 + V_{gq}^2}. \quad (5)$$

157 The error between the reference and the measurement,  $e = V_g^* - V_g$ , passes to a PI controller. This PI 157



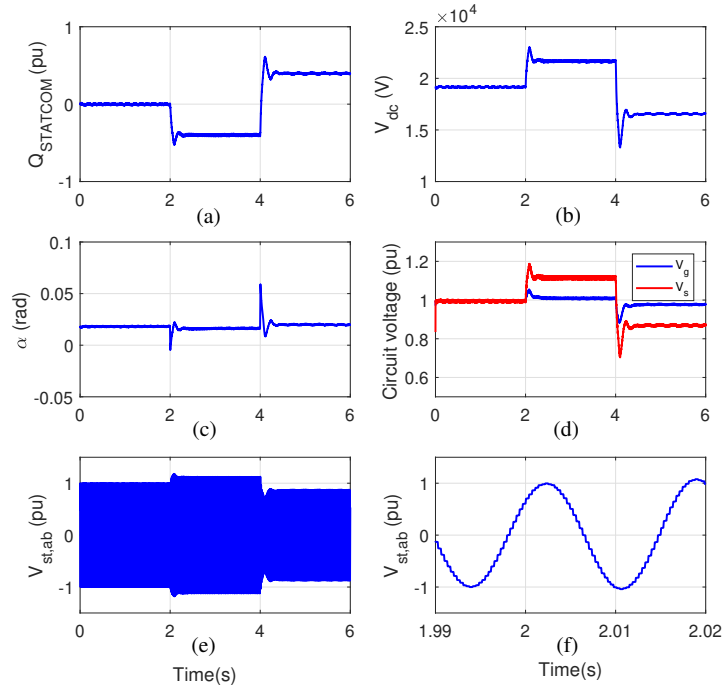


Figure 4: (a) Reactive power from the grid to the STATCOM. (b) STATCOM capacitor voltage. (c) STATCOM terminal voltage angle. (d) Terminal voltages of STATCOM and grid. (e) STATCOM line-to-line voltage. (f) Zoom-in STATCOM line-to-line voltage.

158 controller generates the  $q$ -axis current order  $i_q^*$ . The inner current control employing PI control structure 158  
 159 enforces  $i_q$  to track its order. 159

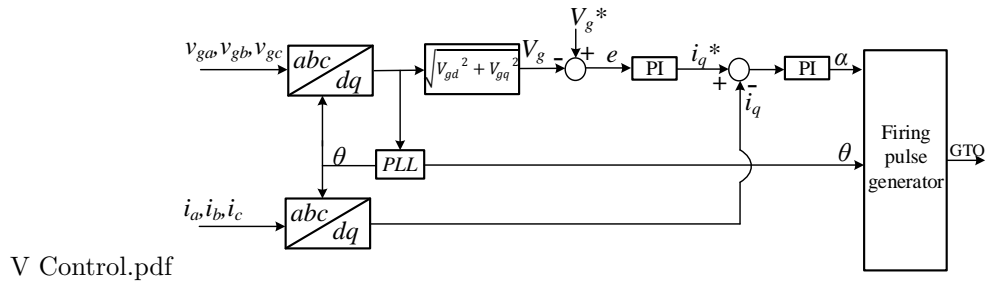


Figure 5: Voltage control block diagram of STATCOM.

160 The parameters of the STATCOM and its controller are listed in Table 2. 160

### 161 2.3. SynCon 161

162 Compared to a STATCOM, a SynCon is a traditional device for reactive power generation and absorption 162  
 163 through electromagnetic field instead of power electronics converters. For a system with limited short-circuit 163

Table 2: Parameters of STATCOM

Parameters	Value (SI)
Rated Power	100 MW
Rated voltage	22 kV
Nominal freq.	60 Hz
DC capacitor	2000 $\mu\text{F}$
$I_q$ PI controller	$5 + \frac{40}{s}$
V PI controller	Para I: $12 + \frac{250}{s}$ Para II: $12 + \frac{100}{s}$
PLL	$60 + \frac{1400}{s}$

164 power capacity, SynCons are usually installed near the generation units to absorb or generate reactive power 164  
 165 and maintain a stable network voltage through excitation control. 165

166 A SynCon essentially is a synchronous machine working under no-load in the motor operation mode. An 166  
 167 excitation system is used to provide excitation current and regulate the terminal voltage for the machine. 167  
 168 According to IEEE standard, there are three different groups of excitation systems: DC type, AC type, and 168  
 169 Static Excitation System (type ST). 169

170 In this model, the SynCon is equipped with a DC2A excitation system as shown in Fig. 6 [23]. At 170  
 171 steady-state, both power system stabilizer voltage  $V_s$  and feedback signal  $V_F$  are zero, which means only 171  
 172 motor terminal voltage  $V_C$  is controlled.  $T_B$  and  $T_C$  are the time constants. The parameters are listed in 172  
 173 Table 3. 173

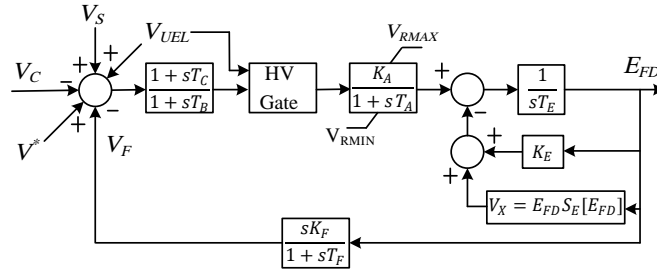


Figure 6: Synchronous condenser exciter model.

## 174 2.4. EMT simulation results 174

### 175 2.4.1. Wind farm only 175

For the 100-MW wind farm grid integration system without any reactive power devices, a dynamic event is created by tripping of a transmission line through a breaker switching. With a closed breaker, the

Table 3: Parameters of synchronous condenser

Parameters	Value (SI)
Rated Power	20 MW
Rated voltage	22 kV
Nominal freq.	60 Hz
$X_d, X'_d, X''_d$	654.4 m $\Omega$ , 99 m $\Omega$ , 79 m $\Omega$
$X_q, X''_q$	629.6 m $\Omega$ , 79.2 m $\Omega$
$R_s, X_{ls}$	1.8 m $\Omega$ , 55.4 m $\Omega$
$T'_{do}, T''_{do}$	4.5 s, 0.04 s
$T'_q, T''_q$	0.67 s, 0.09 s
Inertia constant, p.u.	0.6, 2
Friction factors	0.6
DC capacitor	2000 $\mu$ F
$T_C, T_B$	1, 1
$K_A$	300
$T_E, K_E$	0.01, 2
$K_F$	0.01

impedance of the grid is denoted as:

$$Z_g = (R_1 + jX_1) || (R_2 + jX_2) \quad (6)$$

If the breaker is switched off, the line impedance will be increased as:

$$Z_g = R_1 + jX_1 \quad (7)$$

176 The grid becomes weaker through the breaker's action. 176

177 The wind farm simulation results of the PCC voltage are presented in Fig. 7. It can be observed that the 177  
 178 system becomes unstable when  $X_g$  increases from 0.2 pu to 0.42 pu, while it keeps stable when  $X_g$  increases 178  
 to 0.41 pu. Furthermore, the oscillation frequency of the unstable condition is about 9 Hz.

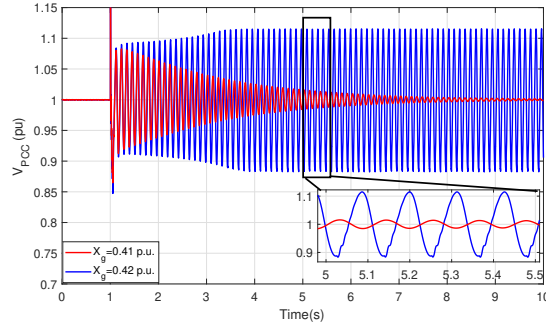


Figure 7: Voltage at PCC bus in wind farm system. The line impedance changes at 1 s.

180 2.4.2. Wind farm with STATCOM

181 To check the effect of STATCOM, the STATCOM operating in reactive power control mode is connected  
 182 to the 22-kV bus. Two cases are simulated. In the first case, there is no active and reactive power transferred  
 183 between the STATCOM and the power system. Fig. 8 presents the waveform of the PCC voltage and  
 184 STATCOM reactive power. It can be noted that the system collapses when  $X_g$  changes from 0.2 pu to 0.42  
 185 pu due to line tripping. As illustrated in the sole wind farm case study, the wind farm marginal stability  
 186 condition is at  $X_g = 0.41$  pu, which means the STATCOM cannot improve the system stability performance  
 187 when there is no reactive power compensation under this control strategy and this set of control parameters.

188 As a comparison, another case is conducted when the STATCOM injects reactive power into the system.  
 189 Fig. 8(b) shows that the oscillations are suppressed if the STATCOM injects 0.1 pu reactive power into the  
 190 system.

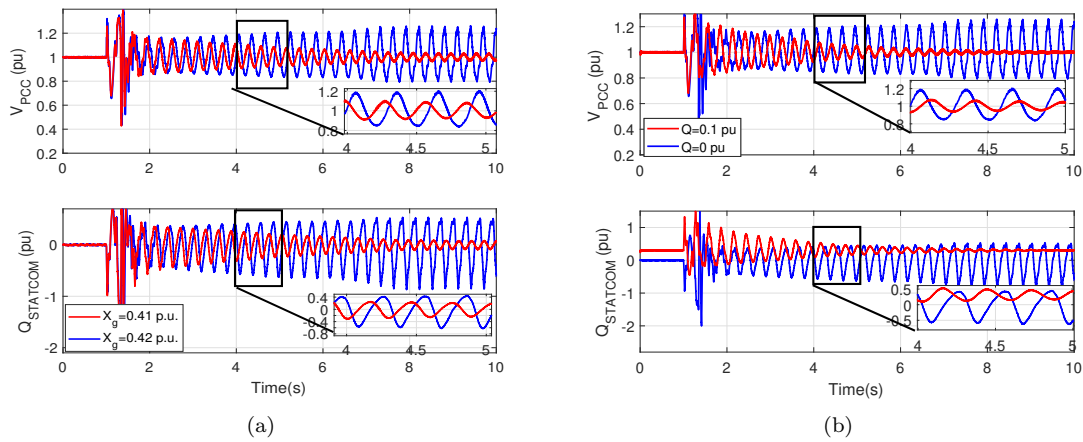


Figure 8: STATCOM in reactive power control mode. (a) Voltage at PCC bus and reactive power from STATCOM. (b) Voltage at PCC bus in wind farm system with STATCOM when  $X_g$  changes to 0.42 pu at 1 second, STATCOM injects 0 or 0.1 pu reactive power to system.

191 Different PI controller parameters are also examined in this control system. The dynamic performance  
 192 comparison is shown in Fig. 9(a). At 1 second, the  $X_g$  increases to 0.42 pu, the larger PI parameter has a  
 193 better stability performance, and the smaller parameters may worsen the oscillation. Fig. 9(b) demonstrate  
 194 the larger PI parameters could increase the marginal stability condition to 0.46 pu.

195 In addition, two additional control modes, fixed firing angle control mode and ac voltage control mode,  
 196 are examined for their impact on STATCOM's stability improvement capability.

197 When the system is working with fixed firing angle control as shown in Fig. 10, the control signal  $\alpha$  is  
 198 set as a constant to ensure reactive power from STATCOM be zero during operation.

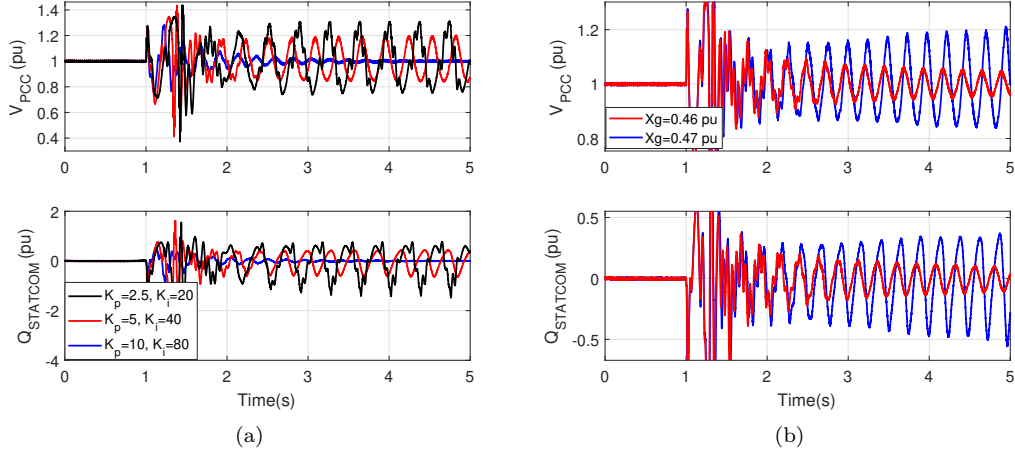


Figure 9: (a) Comparison of different PI controllers at reactive power control mode when  $X_g$  increases to 0.42 pu. (b)  $X_g$  increases to 0.46 pu and 0.47 pu with the PI controller parameters as  $k_p = 10, k_i = 80$ .

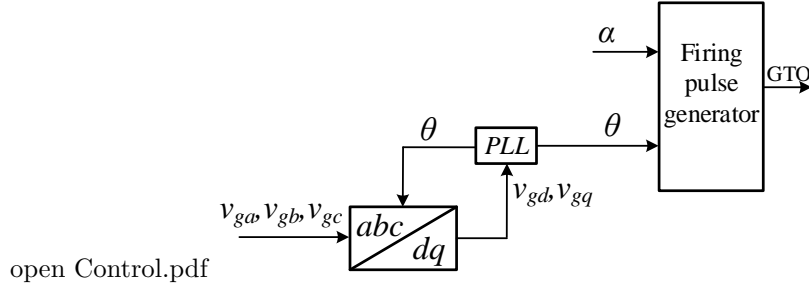


Figure 10: STATCOM fixed firing angle control.

199 Fig. 11(a) shows the system becomes stable when  $X_g$  increases to 0.42 pu with the fixed firing angle 199  
 200 control. Fig. 11(b) shows the fixed firing angle control is able to increase the marginal  $X_g$  to 0.48 pu. When 200  
 201  $X_g$  changes 0.49 pu, the system becomes unstable and oscillation frequency is about 17 Hz. 201

202 When STATCOM is operating at ac voltage control mode, its voltage reference is tuned to maintain 202  
 203 the reactive power from STATCOM zero. Two sets of voltage controller parameters are implemented. Fig. 203  
 204 12(a) shows the simulation results when  $X_g$  increases to 0.41 pu and 0.42 pu with Para I. It can be seen that 204  
 205 the system stability performance is the same with reactive power control. But if the parameters change to 205  
 206 Para II, the system will be stable when  $X_g$  changes to 0.42 pu as shown in Fig. 12(b). Fig. 13 illustrates 206  
 207 the system with Para II could increase the marginal stability condition to 0.49 pu. The oscillation frequency 207  
 208 when  $X_g$  changes to 0.50 pu is about 18 Hz. 208

209 **Remarks:** Through simulation studies of STATCOM in different control modes and different param- 209  
 210 eters, it can be seen STATCOM can improve the stability limit of  $X_g$  from 0.42 pu to 0.49 pu, if proper 210  
 211 control is selected. In some other cases, STATCOM may show zero improvement on stability. 211

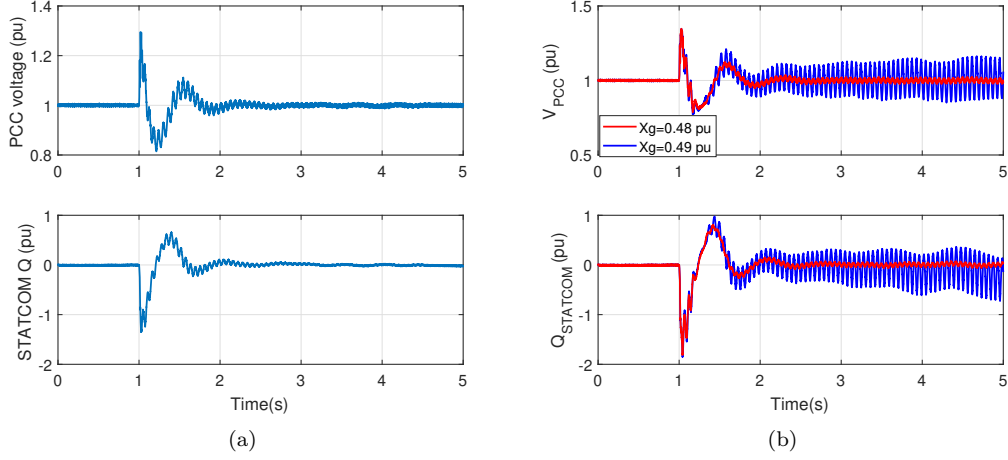


Figure 11: STATCOM with fixed firing angle control. Voltage at PCC bus and the reactive power from the STATCOM when (a)  $X_g$  increases to 0.42 pu. (b)  $X_g$  increases to 0.48 pu and 0.49 pu.

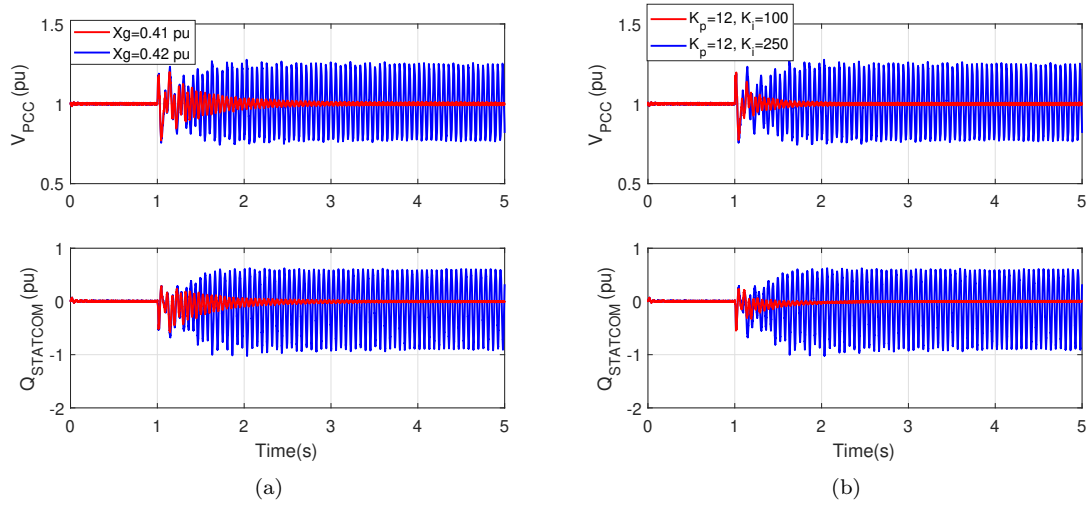


Figure 12: STATCOM in ac voltage control mode. Voltage at PCC bus and the reactive power from the STATCOM when (a)  $X_g$  increases to 0.41 pu and 0.42 pu with Para I. (b)  $X_g$  increases to 0.42 pu with Para I and Para II.

### 212 2.4.3. Wind farm with SynCon 212

213 Finally, the SynCon replaces the STATCOM and operates in parallel with the wind farm. Its generated 213  
 214 power and reactive power are regulated by an excitation system. In this case, the synchronous condenser is 214  
 215 operated under no power condition. 215

216 Fig. 14(a) shows the PCC bus voltage and reactive power from the SynCon when  $X_g$  changes from 0.2 216  
 217 pu to 0.42 pu. After a short period of oscillations, the system recovers to stability. To find out the marginal 217  
 218 stability condition, the transmission line impedance is adjusted. Fig. 14(b) shows the reactive power when 218  
 219  $X_g$  increases to 0.66 and 0.67 pu, which demonstrates the marginal stability condition is  $X_g = 0.66$  pu. The 219

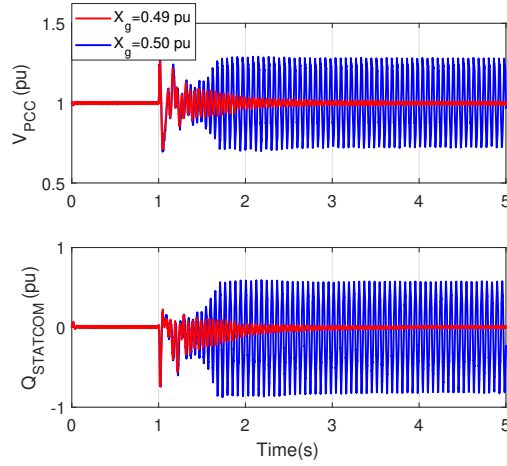


Figure 13: STATCOM in ac voltage control model. Voltage at PCC bus and the reactive power from the STATCOM when  $X_g$  increases to 0.49 pu and 0.50 pu with Para II.

220 cases illustrate that the SynCon can improve the stability performance significantly even without reactive 220  
 221 power compensation. 221

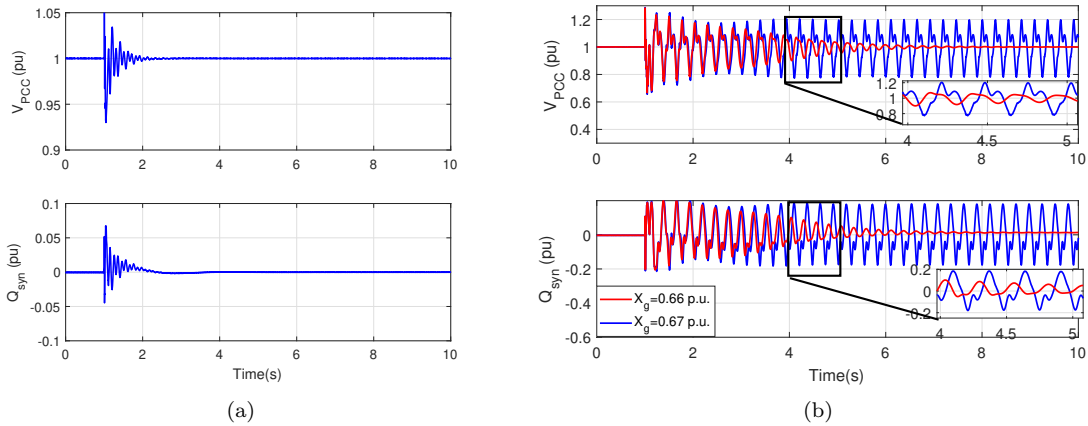


Figure 14: (a) Voltage at PCC bus and synchronous condenser reactive power in wind farm system when  $X_g$  changes from 0.20 to 0.42 pu. (b) Voltage at PCC bus and the reactive power from the SynCon for two additional cases:  $X_g$  changes from 0.20 pu to 0.66 pu and 0.67 pu, respectively .

222 **Remarks:** Although both STATCOM and SynCon have the capability providing reactive power and 222  
 223 improving stability performance due to reactive power supply, SynCon has advantage over STATCOM at 223  
 224 zero reactive power conduction. 224

### 225 3. Admittance-based analysis 225

226 To understand the difference between SynCon and STATCOM in weak grid stability improvement, we 226

227 examine their admittance models. 227

### 228 3.1. Admittance model extraction 228

229 The frequency scanning technique is employed to measure the admittance frequency-domain responses. 229  
 230 The currents and voltages in  $dq$ -domain are recorded after injecting a small-signal perturbation at the 230  
 231 terminal. The obtained data are used to calculate admittance model. 231

232 As Fig. 15 shows, the controllable voltage source is connected to the wind farm at the interconnection 232  
 233 point of 220 kV. Two perturbation voltages are superimposed into the voltage source, respectively. The 233  
 234 voltages are defined in the  $dq$ -frame and converted to the  $abc$ -frame to form a three-phase voltage source. 234  
 235 The resulting currents are recorded at the PCC bus. They are converted to  $dq$ -frame variables  $i_{dq}$ . Fast 235  
 236 Fourier transform (FFT) is implemented to extract the phasor form of  $v_{dq}$  and  $i_{dq}$  at the frequency of the 236  
 237 injected perturbation. It should be noted that the injected perturbation needs to be small enough so it has 237  
 238 no influence on the system operation. 238

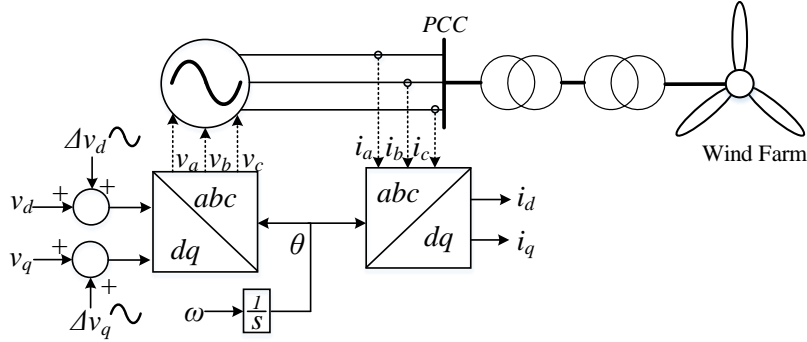


Figure 15:  $Dq$ -frame admittance measurement testbed.

The admittance at every frequency point is calculated as:

$$\begin{aligned}
 Y_{dd}(f_i) &= \frac{i_d^{(1)}(f_i)}{v_d^{(1)}(f_i)} & Y_{dq}(f_i) &= \frac{i_d^{(2)}(f_i)}{v_q^{(2)}(f_i)} \\
 Y_{qd}(f_i) &= \frac{i_q^{(1)}(f_i)}{v_d^{(1)}(f_i)} & Y_{qq}(f_i) &= \frac{i_q^{(2)}(f_i)}{v_q^{(2)}(f_i)}
 \end{aligned} \tag{8}$$

239 where superscripts (1) and (2) are related to voltage perturbation in  $d$ - and  $q$ -axes, respectively;  $f_i$  is the 239  
 240 injected frequency. 240

241 The injection frequencies are swept from 1 to 100 Hz with 1 Hz interval.  $Dq$ -frame voltages and currents 241  
 242 are recorded and processed. FFT window is long enough to reduce the impact of spectral analysis. Fig. 16 242  
 243 shows the wind farm admittance model. Each red plus sign means an injected voltage point. 243



244 The measurements can be fitted to an  $s$ -domain transfer function matrix via the vector fitting toolbox 244  
 245 [13]. The order of the estimated system is firstly to set as 13 for each admittance of  $Y_{dd}$ ,  $Y_{dq}$ ,  $Y_{qd}$  and  $Y_{qq}$ . 245  
 246 Fig. 16 illustrates the comparison of the Bode plot from estimated model (blue line) and measurement data 246  
 247 (red crosses) from harmonic injection. They show high similarity. 247

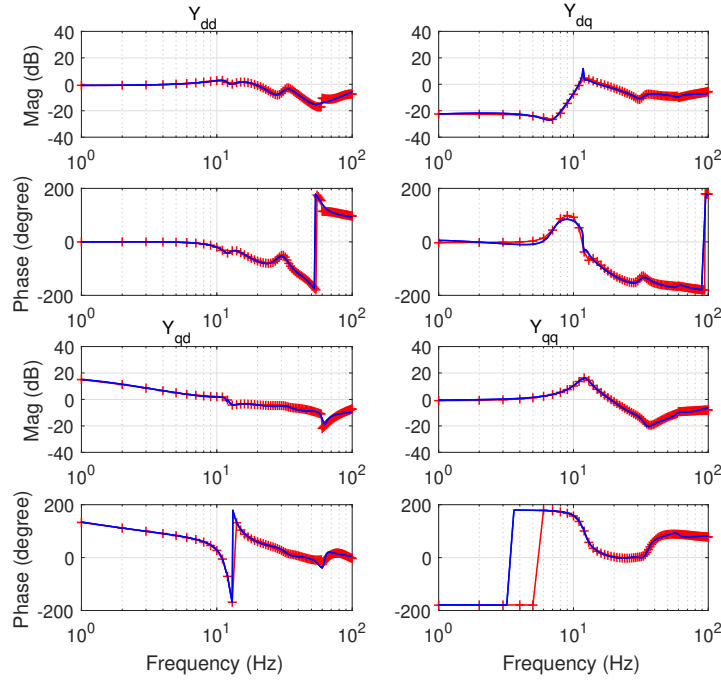


Figure 16: Comparison of the wind farm admittance model from vector fitting and harmonic injection measurement points.

### 248 3.2. Stability analysis 248

This section presents  $s$ -domain admittance based eigenvalue analysis. The wind farm is represented by a Norton equivalent circuit consisting of a current source  $i_{\text{wind}}$  connected with an admittance  $Y_{\text{wind}}$  in parallel. The grid side is also converted to a Norton equivalent circuit with a current source  $i_s$  and line admittance  $Y_{\text{grid}}$ . Thus, from the view of the PCC bus, there are two parallel-connected shunt admittance. At steady state, the system operation condition point is transferred to  $dq$ -frame by using Park transformation. The voltage and current variables in  $dq$ -frame are related as:

$$\begin{bmatrix} i_d \\ i_q \end{bmatrix} = \underbrace{(Y_{\text{wind}} + Y_{\text{grid}})}_Y \begin{bmatrix} v_d \\ v_q \end{bmatrix} \quad (9)$$

where

$$Y_{\text{wind}} = \begin{bmatrix} Y_{dd} & Y_{dq} \\ Y_{qd} & Y_{qq} \end{bmatrix}, Y_{\text{grid}} = \begin{bmatrix} R_g + sL_g & -\omega_o L_g \\ \omega_o L_g & R_g + sL_g \end{bmatrix}$$

where  $\omega_o$  is the nominal frequency.

If the system is regarded as an input/output system, where the injected current and the PCC voltage are denoted as the input and the output, respectively, then the transfer function  $G(s)$  for the multi-input multi-output (MIMO) system is  $Y(s)^{-1}$ . The closed-loop system eigenvalues, or the poles of  $G(s)$ , are the roots of  $\det(Y(s))$  according to [11]. With the admittance of the wind farm being identified from measurements, the eigenvalues of the entire system can be found if the transmission line parameters are known.

Furthermore, when a reactive power device is employed in the system, then the overall admittance is:

$$Y = Y_{\text{wind}} + Y_{\text{grid}} + Y_{\text{shunt}} \quad (10)$$

where  $Y_{\text{shunt}}$  is the admittance model of the SynCon or STATCOM.

The  $s$ -domain model from vector fitting can be used for eigenvalue analysis.

### 3.2.1. Wind farm only

According to (10), the eigenvalue loci are plotted in Fig. 17(a) with known  $Y_{\text{wind}}$ , and  $Y_{\text{grid}}$  has an increment of 0.01 pu from 0.3 pu to 0.5 pu.

It can be observed that there is one pair of complex conjugate mode affected by the varying impedance. When  $X_g$  is 0.42 pu, the oscillation mode at 9 Hz moves to right half plane (RHP), which corroborates with the simulation results shown in Fig. 7.

### 3.2.2. Wind farm with STATCOM

The STATCOM model is identified using harmonic injection method when it is operated in reactive power control with parameters listed in Table 2. The frequency is swept from 1 to 200 Hz with an interval of 1 Hz. Afterwards, the  $dq$ -admittance measurements of 200 points are obtained and processed by vector-fitting algorithm to arrive at the linear model  $Y_{\text{STATCOM}}$  in  $s$ -domain.

Fig. 17(b) shows the movements of the dominant zeros of  $Y_{\text{STATCOM}} + Y_{\text{wind}} + Y_{\text{grid}}$ , as  $X_g$  varying from 0.3 pu to 0.5 pu. It is evident that one pair of eigenvalues crosses the imaginary axis when  $X_g$  increases to 0.42 pu, which corroborates the EMT simulation results of Fig. 8.

272 Similar to the STATCOM, the SynCon is also measured for its admittance model  $Y_{\text{syn}}$  in range of 1 to 272  
 273 200 Hz. Fig. 17(c) shows the Eigen Loci of the overall system when  $X_g$  is changed from 0.6 to 0.8 pu. It can 273  
 274 be observed that a pair of eigenvalues move to the RHP when  $X_g$  reaches 0.67 pu. This analytical analysis 274  
 275 corroborates the EMT simulation results. 275

### 276 3.3. Comparison of admittance of STATCOM and SynCon 276

277 Fig. 18 presents the  $dq$ -domain admittance models of the SynCon and STATCOM. It should be mentioned 277  
 278 that both the two models have the same operating condition in the wind farm system. 278

To have a better understanding, we resort to a different domain. The admittance model can be expressed in different domains, e.g., sequence domain or  $dq$ -frame. The two types of models are related [24]:

$$\begin{bmatrix} Y_{pp} & Y_{pn} \\ Y_{np} & Y_{nn} \end{bmatrix} = \frac{1}{2} \begin{bmatrix} 1 & j \\ 1 & -j \end{bmatrix} \begin{bmatrix} Y_{dd} & Y_{dq} \\ Y_{qd} & Y_{qq} \end{bmatrix} \begin{bmatrix} 1 & 1 \\ -j & j \end{bmatrix} \quad (11)$$

The sequence-domain admittance associates the two current phasors and two voltage phasors. The two voltage (current) phasors are referred to the phasors at positive-sequence at frequency  $\omega_p + \omega_1$  and negative-sequence at frequency  $\omega_p - \omega_1$ , where  $\omega_1$  is the nominal frequency of 60 Hz.

$$\begin{bmatrix} \bar{I}_p(j(\omega_p + \omega_1)) \\ \bar{I}_n(j(\omega_p - \omega_1)) \end{bmatrix} = \begin{bmatrix} Y_{pp}(j\omega_p) & Y_{pn}(j\omega_p) \\ Y_{np}(j\omega_p) & Y_{nn}(j\omega_p) \end{bmatrix} \begin{bmatrix} \bar{V}_p(j(\omega_p + \omega_1)) \\ \bar{V}_n(j(\omega_p - \omega_1)) \end{bmatrix} \quad (12)$$

Combining equation (11) and (12), the sequence-based current is related to voltage through  $dq$ -admittance as:

$$\begin{bmatrix} \bar{I}_p \\ \bar{I}_n \end{bmatrix} = \frac{1}{2} \begin{bmatrix} 1 & j \\ 1 & -j \end{bmatrix} \begin{bmatrix} Y_{dd} & Y_{dq} \\ Y_{qd} & Y_{qq} \end{bmatrix} \begin{bmatrix} 1 & 1 \\ -j & j \end{bmatrix} \begin{bmatrix} \bar{V}_p \\ \bar{V}_n \end{bmatrix} \quad (13)$$

279 At steady-state, the operation condition is at 60 Hz, so the  $dq$ -domain admittance at 0 Hz will be 279  
 280 analyzed. From the Bode plot, it can be observed that the steady-state admittance is at the leftmost 280  
 281 frequency range. 281

The Bode plot indicates that the magnitude of  $Y_{dd}$ ,  $Y_{dq}$  and  $Y_{qq}$  in synchronous condenser are relatively small compared to  $Y_{qd}$  at steady state, thus they can be approximated to zero. The magnitude of  $Y_{qd}$  is found as -6 dB or 0.5 pu. Similarly, the magnitude of  $Y_{dd}$ ,  $Y_{dq}$  and  $Y_{qq}$  in STATCOM are treated as zero

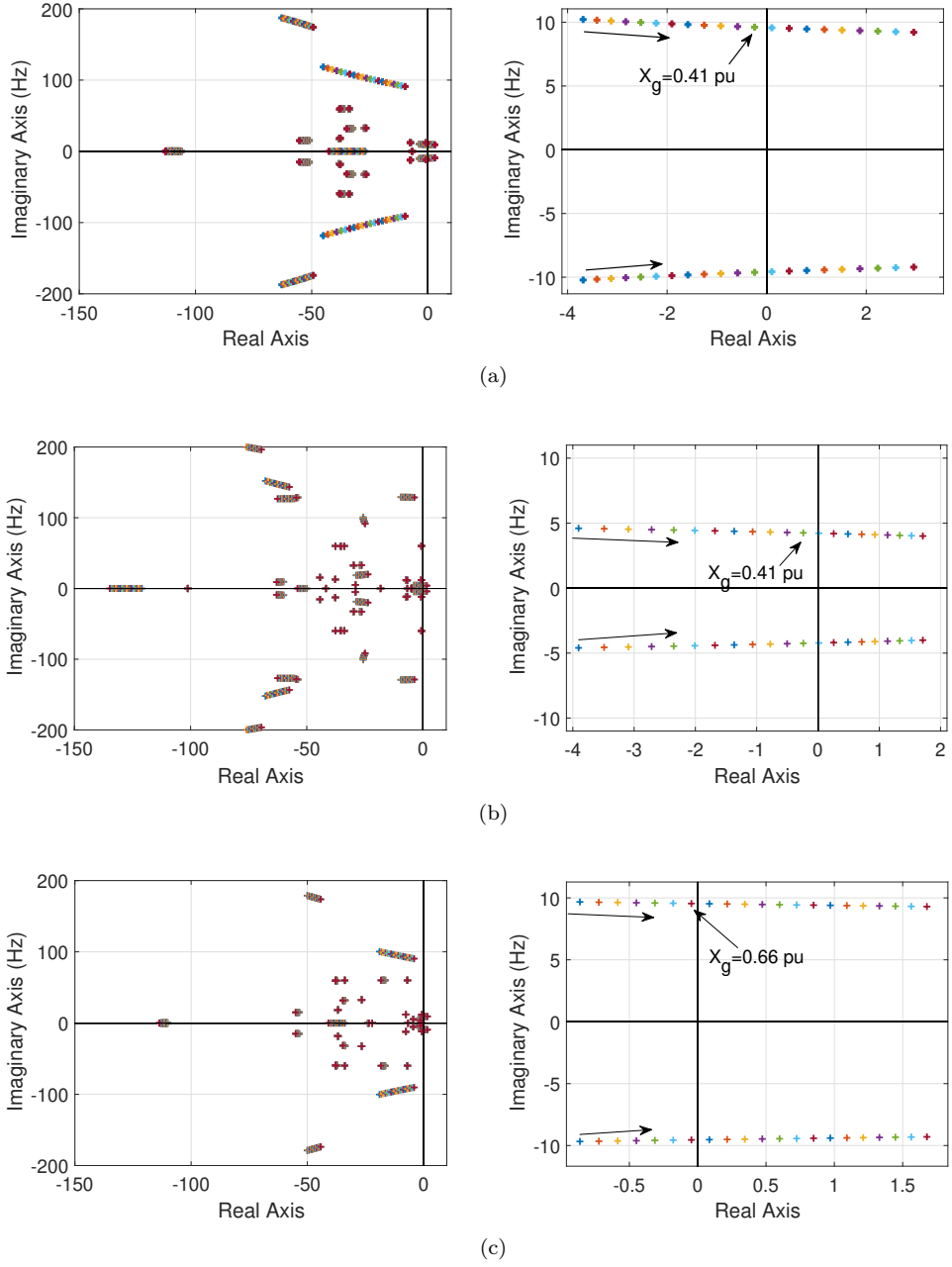


Figure 17: Eigen loci for varying line impedance  $X_g$  for (a) wind farm, (b) wind farm with STATCOM, and (c) wind farm with SynCon. The right plots are the zoom-in of the left plots at critical mode.

and  $Y_{qq}$  is -10 dB or 0.3 pu. Then we can conclude the  $dq$ -domain admittance models at steady-state as:

$$\mathbf{Y}_{\text{syn,dq}} = \begin{bmatrix} 0 & 0 \\ -0.5 & 0 \end{bmatrix}, \quad \mathbf{Y}_{\text{st,dq}} = \begin{bmatrix} 0 & 0 \\ 0 & -0.3 \end{bmatrix} \quad (14)$$

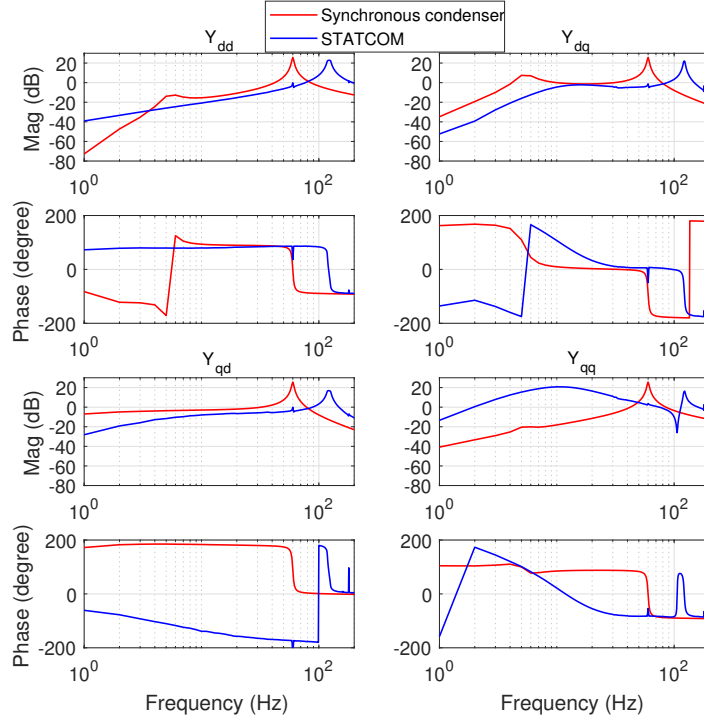


Figure 18:  $Dq$ -domain admittance comparison of synchronous condenser and STATCOM.

282 Assuming the system is balanced, positive and negative-sequence voltage are  $1\angle 0^\circ$  and 0, respectively. 282

For SynCon, the only non-zero element is  $Y_{qd}$  at 0 Hz, hence:

$$\begin{bmatrix} \bar{I}_p \\ \bar{I}_n \end{bmatrix} = \frac{jY_{qd}}{2} \begin{bmatrix} 1 & 1 \\ -1 & -1 \end{bmatrix} \begin{bmatrix} \bar{V}_p \\ \bar{V}_n \end{bmatrix} \quad (15)$$

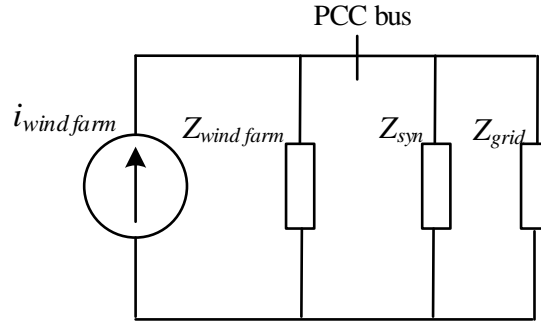
$$\Rightarrow \bar{I} = \bar{I}_p + \bar{I}_n^* = jY_{qd}\bar{V}_p = -j0.5\bar{V}_p = \frac{1}{j2}\bar{V}_p \quad (16)$$

283 Hence, the SynCon can be regarded as an impedance connected in parallel with PCC bus. As shown in 283  
 284 Fig. 19, by adding a parallel branch, the impedance after PCC bus will be reduced and the grid strength is 284  
 285 improved. This is the reason why SynCon can improve stability even without injecting any reactive power. 285

Similarly, for the STATCOM, the sequence-domain admittance is expressed as follows.

$$\begin{bmatrix} \bar{I}_p \\ \bar{I}_n \end{bmatrix} = \frac{1}{2} \begin{bmatrix} Y_{qq} & -Y_{qq} \\ -Y_{qq} & Y_{qq} \end{bmatrix} \begin{bmatrix} \bar{V}_p \\ \bar{V}_n \end{bmatrix} \quad (17)$$

$$\Rightarrow \bar{I} = \bar{I}_p + \bar{I}_n^* = \left( \frac{1}{2}Y_{qq} - \frac{1}{2}Y_{qq} \right) \bar{V}_p = 0 \cdot \bar{V}_p \quad (18)$$



circuit.pdf

Figure 19: Equivalent circuit model of a wind farm connected with a SynCon.

This result implies that the STATCOM does not provide an impedance in the circuit and acts as a current source at steady state or low-frequency range. Thus, the grid impedance remains the same and the stability is not improved.

**Remarks:** Through examining  $dq$ -frame admittances of a SynCon and a STATCOM, it is found that the two differ in providing (or not providing) a reactance at steady state. This difference causes the difference in stability enhancement.

#### 4. Conclusion

As the mostly used reactive power devices, SynCon and STATCOM are implemented in a type-4 wind farm system to investigate their impacts on the overall stability of the system. It has been shown that both the SynCon and the STATCOM can improve the system stability performance without reactive power compensation. On the other hand, SynCon can improve the stability margin more significantly than STATCOM. If not tuned properly, STATCOM may show zero stability improvement. This paper gives an explanation of this phenomenon based on their frequency-domain admittance models. The frequency-domain measurements are obtained from harmonic injection, and the measurement data are fitted into  $s$ -domain models through vector fitting method. Eigenvalue analysis results confirm the observation from the EMT simulation. It is found that SynCon and STATCOM differ in  $dq$ -frame admittance at low-frequency range significantly. The difference also demonstrates as SynCon providing a shunt reactance at steady state while STATCOM providing zero impedance at steady state. This equivalent impedance provided by SynCon helps increase the grid strength to allow more transferred power and enhanced stability.

- [1] IEEE PES WindSSO Taskforce, PES TR-80: Wind Energy Systems Subsynchronous Oscillations: Events and Modeling, 2020.
- [2] L. Fan, Z. Miao, An explanation of oscillations due to wind power plants weak grid interconnection, IEEE trans. Sustainable Energy 9 (1) (2018) 488–490.
- [3] Y. Li, L. Fan, Z. Miao, Stability control for wind in weak grids, IEEE Trans. Sustainable Energy 10 (4) (2019) 2094–2103.
- [4] J. Liston, Typical synchronous condenser installations, General Electric Company Review 14 (1911) 234–241.
- [5] 2018 state of the market report for the ERCOT electricity markets (2019).

- 312 [6] J. Skliutas, D. LaForest, R. D'Aquila, D. Derr, E. Kronbeck, Next-generation synchronous condenser installation at the 312  
313 velco granite substation, in: 2009 IEEE Power Energy Society General Meeting, 2009, pp. 1–8. doi:10.1109/PES.2009. 313  
314 5275396. 314
- 315 [7] B. Singh, R. Saha, A. Chandra, K. Al-Haddad, Static synchronous compensators (statcom): a review, IET Power Elec- 315  
316 tronics 2 (4) (2009) 297–324. 316
- 317 [8] G. Reed, J. Paserba, T. Croasdaile, M. Takeda, Y. Hamasaki, T. Aritsuka, N. Morishima, S. Jochi, I. Iyoda, M. Nambu, 317  
318 N. Toki, L. Thomas, G. Smith, D. LaForest, W. Allard, D. Haas, The velco statcom based transmission system project, 318  
319 in: 2001 IEEE Power Engineering Society Winter Meeting. Conference Proceedings (Cat. No.01CH37194), Vol. 3, 2001, 319  
320 pp. 1109–1114 vol.3. doi:10.1109/PESW.2001.917226. 320
- 321 [9] A. Hoke, V. Gevorgian, S. Shah, P. Koralewicz, R. W. Kenyon, B. Kroposki, Island power systems with high levels of 321  
322 inverter-based resources: Stability and reliability challenges, IEEE Electrification Magazine 9 (1) (2021) 74–91. doi: 322  
323 10.1109/MELE.2020.3047169. 323
- 324 [10] The age of the syncons, <https://www.energynetworks.com.au/news/energy-insider/age-syncons/>, accessed: 2021-09-02 324  
325 (2019). 325
- 326 [11] A. I. Semlyen, s-domain methodology for assessing the small signal stability of complex systems in nonsinusoidal steady 326  
327 state, IEEE Transactions on Power Systems 14 (1) (1999) 132–137. doi:10.1109/59.744501. 327
- 328 [12] L. Fan, Z. Miao, Admittance-based stability analysis: Bode plots, nyquist diagrams or eigenvalue analysis?, IEEE Trans- 328  
329 actions on Power Systems 35 (4) (2020) 3312–3315. doi:10.1109/TPWRS.2020.2996014. 329
- 330 [13] B. Gustavsen, A. Semlyen, Rational approximation of frequency domain responses by vector fitting, IEEE Transactions 330  
331 on Power Delivery 14 (3) (1999) 1052–1061. doi:10.1109/61.772353. 331
- 332 [14] L. Ljung, R. Singh, Version 8 of the matlab system identification toolbox, IFAC Proceedings Volumes 45 (16) (2012) 332  
333 1826–1831. 333
- 334 [15] J. Dixon, L. Moran, J. Rodriguez, R. Domke, Reactive power compensation technologies: State-of-the-art review, Pro- 334  
335 ceedings of the IEEE 93 (12) (2005) 2144–2164. doi:10.1109/JPROC.2005.859937. 335
- 336 [16] Y. Zhang, A. M. Gole, Comparison of the transient performance of statcom and synchronous condenser at hvdc converter 336  
337 stations, in: 11th IET International Conference on AC and DC Power Transmission, 2015, pp. 1–8. doi:10.1049/cp. 337  
338 2015.0069. 338
- 339 [17] Y. Liu, S. Yang, S. Zhang, F. Z. Peng, Comparison of synchronous condenser and statcom for inertial response support, in: 339  
340 2014 IEEE Energy Conversion Congress and Exposition (ECCE), 2014, pp. 2684–2690. doi:10.1109/ECCE.2014.6953761. 340
- 341 [18] C. Li, R. Burgos, B. Wen, Y. Tang, D. Boroyevich, Analysis of statcom small-signal impedance in the synchronous d-q 341  
342 frame, IEEE Journal of Emerging and Selected Topics in Power Electronics 8 (2) (2020) 1894–1910. doi:10.1109/JESTPE. 342  
343 2019.2942332. 343
- 344 [19] C. Li, R. Burgos, Y. Tang, D. Boroyevich, Application of d-q frame impedance-based stability criterion in power systems 344  
345 with multiple statcoms in proximity, in: IECON 2017 - 43rd Annual Conference of the IEEE Industrial Electronics Society, 345  
346 2017, pp. 126–131. doi:10.1109/IECON.2017.8216026. 346
- 347 [20] L. Bao, L. Fan, Z. Miao, Comparison of synchronous condenser and STATCOM for wind farms in weak grids, NAPS 2020. 347  
348 [21] MATLAB, Statcom (detailed model). 348  
349 URL [https://www.mathworks.com/help/physmod/sps/ug/statcom-detailed-model.html;jsessionid=](https://www.mathworks.com/help/physmod/sps/ug/statcom-detailed-model.html;jsessionid=2a1b35ac24097edc871901940247) 349  
350 [2a1b35ac24097edc871901940247](https://www.mathworks.com/help/physmod/sps/ug/statcom-detailed-model.html;jsessionid=2a1b35ac24097edc871901940247) 350

- 351 [22] N. G. Hingorani, L. Gyugyi, *Static Shunt Compensators: SVC and STATCOM*, 2000, pp. 135–207. doi:10.1109/ 351  
352 9780470546802.ch5. 352
- 353 [23] IEEE Recommended Practice for Excitation System Models for Power System Stability Studies, IEEE Std 421.5-1992 353  
354 (1992) 1–56. 354
- 355 [24] A. Rygg, M. Molinas, C. Zhang, X. Cai, A modified sequence-domain impedance definition and its equivalence to the 355  
356 dq-domain impedance definition for the stability analysis of ac power electronic systems, *IEEE Journal of Emerging and 356*  
357 *Selected Topics in Power Electronics* 4 (4) (2016) 1383–1396. doi:10.1109/JESTPE.2016.2588733. 357